Typeset with jjap2.cls <ver.1.1> **Regular Paper**

Nucleation-fibrillation dynamics of Aβ_{1-40} peptides on liquid-solid surface studied by total-internal-reflection fluorescence microscopy coupled with quartz-crystal microbalance biosensor

Hiroki HAMADA[1], Hirotsugu OGI[1]*, Kentaro NOI[2], Hisashi YAGI[3], Yuji GOTO[4], and Masahiko HIRAO[1]

[1]*Graduate School of Engineering Science, Osaka University, Toyonaka, Osaka 560-8531, Japan*
[2]*Institute of Molecular Embryology and Genetics, Kumamoto University, Kumamoto 860-0811, Japan*
[3]*Center for Research on Green Sustainable Chemistry, Tottori University, Tottori 680-8550, Japan*
[4]*Institute for Protein Research, Osaka University, Suita, Osaka 565-0871, Japan*

We have successfully developed the total-internal-reflection-fluorescence microscopy combined with a quartz-crystal microbalance (TIRFM-QCM) biosensor, and monitored the nucleation-fibrillation phenomenon of amyloid β_{1-40} peptide on the naked quartz surface. The cross-β-sheet structures were visualized with the TIRFM using the thioflavin-T (Th-T) label, and other unlabeled aggregates were detected through the frequency change of the 58-MHz wireless-electrodeless QCM throughout the aggregation reaction. The QCM response indicates significant adsorption of the peptides on the quartz surface at the early stage, which is followed by fibrillation. The non-cross-β-sheet oligomers are first formed, and nuclei appear in the oligomer region, from which fibrils originate and elongate. The two-color TIRFM observation was performed after the aggregation reaction with the Nile-red label as well as the ThT label for identifying nucleation from non-β-sheet regions. An aggregation model is proposed.

1. Introduction

Alzheimers disease (AD) is deeply associated with assembly of Aβ peptides, the amyloidogenic peptides, which accumulate in human brain, exhibiting neurotoxicity to cause AD.[1,2)] Despite significant efforts paid for clarifying the pathogenic mechanism of AD,[3–10)] the aggregation behavior of Aβ peptides still remains unclear. One reason will be that there are few studies covering throughout aggregation process from nucleation to fibril elongation on the liquid-solid surface. As seen in the previous reports, Aβ peptides form seeds on the cell membrane, on which the peptides cause significant deposition for creating amyloid fibrils.[11,12)] Thus, monitoring the aggregation reaction on liquid-solid surface is a critical issue. Conventional methods used total internal reflection microscopy (TIRFM)[13–15)] or atomic force microscopy (AFM)[16–18)] for monitoring single fibril elongation behavior. However, TIRFM fails to observe growth of unlabeled structures, and AFM fails to cover a long term for the

*E-mail:ogi@me.es.osaka-u.ac.jp

throughout monitoring of aggregation reaction. They were furthermore performed in non-flow conditions, which drastically deteriorate reaction constants.[19)]

We recently developed the TIRFM-QCM system,[20)] which monitors the aggregation reaction of the Aβ peptides on the naked AT-cut quartz plate via TIRFM and QCM simultaneously: Formation of any aggregates, including unlabeled aggregates, can be detected through the frequency change of the quartz resonator, and the direct observation of nucleation and elongation of fibrils are made with TIRFM. Thus, this is the only system that monitors progress of the aggregation reaction involving oligomers and fibrils on the liquid-solid surface in real time.

There are two principal Aβ peptides, Aβ_{1-40} and Aβ_{1-42}, consisting of 40 and 42 amino acids, respectively. The former is predominantly produced in vivo,[3)] while Aβ_{1-42} peptide shows higher hydrophobicity than Aβ_{1-40} peptide[21)] and is easily self-assembled to form a seed for fibrillation. In the previous study,[20)] we therefore investigated the fibrillation phenomenon of Aβ_{1-40} peptides on the Aβ_{1-42} seeds and revealed that the fibril formation occurs dramatically in later stages. However, nucleation and elongation of fibrils caused by Aβ_{1-40} seeds are also important because of the larger amount of Aβ_{1-40} peptides in the brain, which could govern the pathogenic mechanism of AD.

Here, we then investigate nucleation and fibrillation behaviors of Aβ_{1-40} peptides on their homogenous seeds using the TIRFM-QCM. We show that fibrillation occurs from an early stage after adsorption of oligomers with non-cross-β-sheet structures.

2. Methods

2.1 Materials and preparation of solutions

The lyophilized Aβ_{1-40} peptides were purchased from Peptide Institute (No. 4307-v). The acetate buffer solution (ABS) with pH4.6 containing 0.1 M NaCl was prepared by mixing 0.1 M acetate acid aqueous solution and 0.1 M sodium acetate aqueous solution. Ultrapure water, sodium chloride acetate acid, sodium acetate, dimethyl sulfoxide (DMSO), and Th-T were purchased from Wako Pure Chemical Industries. Nile red was purchased from Sigma Aldrich.

The Aβ_{1-40} seed solution was prepared as follows. The lyophilized peptide was dissolved by DMSO and diluted into 50 μM with the ABS. This solution was stirred at a rate of 1200 rpm for 6h for making the cross-β-sheet aggregates and sonicated at 200 kHz for obtaining seed fragments. This seed solution was used for immobilization of the Aβ_{1-40} seeds on the quartz surface.

The Aβ_{1-40} monomer solution for flow was prepared as follows. The lyophilized peptide was dissolved by DMSO and diluted with ultrapure water containing Th-T and NaCl. Final concentrations of Aβ_{1-40}, Th-T, and NaCl in the flowing solution are 10 μM, 10 μM, and 100 mM, respectively (DMSO : ultrapure water = 1:19). The running buffer was identical as the

monomer solution, but it does not contain the Aβ_{1-40} peptides.

The Nile-red solution was prepared by dissolving Nile red in acetone for obtaining 1 mM Nile-red/acetone solution, and it was diluted by ultrapure water to obtain the final concentration of 10 μM Nile-red solution.

2.2 TIRFM-QCM system

Figure 1 illustrates the cross-section of the laboratory-built TIRFM-QCM cell. The rectangular parallelepiped AT-cut quartz-crystal resonator (2.0x1.7x0.0285 mm^3) with the fundamental resonance frequency of 58 MHz is located on a 0.15-mm-thick cover glass and held lightly by a 1-mm-thick silicon-rubber sheet, where a rectangular flow path is composed. Two line antennas made of copper are set outside the flow channel for transmitting and receiving the shear vibration of the resonator through electromagnetic waves contactlessly.[22,23] Because the in-plane electric filed is used for the coupling, the in-plane orientation of the resonator is adjusted to make the maximum transmission efficiency. The evanescent field is created over the quartz resonator by the objective lens beneath the cover glass through an immersion oil. The labeled aggregates are detected with the TIRFM.

2.3 Fluorescence methods

We principally used the Th-T fluorescence method for TIRFM during the aggregation reaction on the quartz resonator. Th-T molecules specifically recognize and bind cross-β-sheet structures of Aβ aggregates, including seeds and fibrils, and by absorbing a light near 450 nm, they emit a strong fluorescence near 490 nm. We used the exciting light of 440 nm and detected the fluorescence at 483 nm.

While Th-T shows high specificity to β-sheet structures, it fails to find other oligomeric aggregates without the β-sheet structures. We then adopted the Nile-red fluorescence measurement after the aggregation reaction. Nile red emits fluorescence at 637 nm when it binds lipid-rich portion by adsorbing 553 nm light. It is expected to indicate oligomers without the cross-β sheet as well as fibrils,[24,25] although its fluorescence intensity is lower than that of Th-T.

2.4 Experimental procedure

The naked quartz resonator was washed in a piranha solution (98% H_2SO_4: 33% H_2O_2 =7:3) for 30 min, rinsed with ultrapure water, and cleaned by a UV-ozone cleaner. It was immersed in the Aβ-seed solution for 6 h to immobilize the Aβ_{1-40} seeds on the surface. The resonator was then set in the TIRFM-QCM cell, and the buffer solution was flowed. After the baseline of the resonance frequency became stable, we flowed the monomer solution and monitored the frequency change from QCM and fluorescence images from TRFM.

3. Results and discussion

Figure 2 shows the TIRFM-QCM result. The resonance frequency of the quartz resonator markedly decreases just after the start of the monomer-solution flow, indicating adsorption of the Aβ_{1-40} peptides on the surface. However, number and structure of aggregates appear to be unchanged with TIRFM images in this period ($<\sim$1 h). This observation highly indicates that the Aβ_{1-40} peptides are effectively captured by the surface seeds, and they form non-β-sheet oligomers, which are Th-T negative and invisible with TIRFM.

The peptide deposition reaction rate becomes lower and fibrillation is clearly observed after 2 h. We expect nucleation from the surface oligomers in this stage, from which fibrils originate. Figure 3 compares the TIRFM images at 0 and 5 h to display origins of fibrils. The merged figure (Fig. 3(c)) shows that some fibrils originate from initially immobilized seeds (pointed by arrows), but most fibrils appear from the seed-free area, indicating that nucleation and growth of fibrils principally occur inside the oligomers formed in the early stage. This behavior is different from the aggregation reaction on the heterogenous seeds of Aβ_{1-42},[20] where the fibrillation phenomenon occurs in a later stage ($>\sim$5 h). Because the Aβ_{1-40} seeds are identical as the templates for Aβ_{1-40} fibrils, the formed oligomer structures will be close to those of fibril nucleus, possessing a lower energy barrier for nucleation from them. However, the Aβ_{1-42} seeds will cause oligomers whose structures are significantly different from the nuclei, leading to the delayed nucleation and fibrillation. Such an extended reaction for fibril formation with the presence of heterogenous seeds was also reported for bulk-solution experiments.[26]

To investigate the fibril origin in more detail, we performed a two-color TIRFM measurement using Nile red as well as Th-T. Nile red binds to hydrophobic residue of Aβ aggregates and can identify oligomeric aggregates as well as fibrils. Although Th-T molecules rapidly bind to fibrils, it takes longer time for Nile-red molecules to fully bind aggregates. We therefore dyed the aggregates with Nile red for 1 h after the monomer-solution flow measurement. Figure 4 shows the result. Many fibrils originate from the Nile-red-positive points (Fig. 4(c)), which we consider as β-sheet-poor regions. Because Th-T molecules have attached to the β-sheet structures and occupied their binding sites, few sites have remained for Nile-red molecules. Therefore, they predominantly bind to remaining binding sites, the non-β-sheet structures. Thus, Figure 4(c) supports our view that nucleation occurs from oligomers formed in the early stage, and fibrils mainly elongate from the nuclei rather than initially immobilized seeds.

Here, we propose an aggregation model at the liquid-solid surface as illustrated in Fig. 5. The monomer-solution flow generates oligomers consisting of non-β-sheet structures near the immobilized seed (Fig. 5(b)). During this period, the resonance frequency drastically decreases because many peptides participate in their formation. The nuclei are then produced in the oligomer region (Fig. 5(c)), from which the fibrils originate to grow (Fig. 5(d)).

4. Conclusions

We throughout monitored the aggregation reaction Aβ_{1-40} peptides and their structural change at liquid-solid surface. The formation of oligomer is the key for nucleation and fibrillation, and it was confirmed with the combination of QCM measurement and TIRFM measurement. The fibrillation occurs mainly from the newly created nuclei rather than initially immobilized seeds. Thus, the immobilized seeds enhance the oligomer formation on the surface. Without the electrodeless QCM measurement, this important observation would have remained undiscovered. The TIRFM-QCM system will be thus powerful tool for studying various interactions among proteins and cells.

Acknowledgement

This study was supported by the Funding Program for Next Generation World-Leading Researchers by the Cabinet Office, Government of Japan.

References

1) M. Bucciantini, E. Giannoni, F. Chiti, F. Baroni, L. Formigli, J. Zurdo, N. Taddei, G. Ramponi, C. M. Dobson, M. Stefani: Nature **416** (2002) 507.

2) F. M. LaFerla, K. N. Green, and S. S. Oddo: Nat. Rev. Neurosci. **8** (2007) 499.

3) J. T. Jarrett, E. P. Berger, and P. T. Jr. Lansbury: Biochemistry **32** (1993) 4693.

4) S. J. Wood, B. Maleeff, T. Hart, and R. J. Wetzel: J. Mol. Biol. **256** (1996) 870.

5) G. Bitan, M. D. Kirkitadze, A. Lomakin, S. S. Vollers, G. B. Benedek, and D. B. Teplow: Proc. Natl. Acad. Sci. U.S.A. **100** (2003) 330.

6) H. Ogi, Y. Fukunishi, T. Yanagida, H. Yagi, Y. Goto, M. Fukushima, K. Uesugi, and M. Hirao: Anal. Chem. **83** (2011) 4982.

7) H. Ogi, M. Fukushima, K. Uesugi, H. Yagi, Y. Goto, and M. Hirao, Biosens. Bioelectron. **40** (2013) 200.

8) K. Uesugi, H. Ogi, M. Fukushima, M. So, H. Yagi, Y. Goto, and M. Hirao: Jpn. J. Appl. Phys. **52** (2013) 07HE10.

9) Y. Yoshimura, Y. Lina, H. Yagia, Y. Lee, H. Kitayama, K. Sakurai, M. So, H. Ogi, H. Naiki, and Y. Goto: Proc. Natl. Acad. Sci. U. S. A **109** (2012) 14446.

10) Y. Yoshimura, M. So, H. Yagi, and Y. Goto: Jpn. J. Appl. Phys. **52** (2013) 07HA01.

11) A. Kakio, S. Nishimoto, K. Yanagisawa, Y. Kozutsumi, and K. Matsuzaki: Biochemistry **41** (2002) 7385.

12) C. M. Yip, A. A. Darabie, and J. McLaurin: J. Mol. Biol. **318** (2002) 97.

13) T. Ban, M. Hoshino, S. Takahashi, D. Hamada, K. Hasegawa, H. Naiki, and Y. Goto: J. Mol. Biol. **344** (2004) 757.

14) S. M. Patil, A. Mehta, S. Jha, and A. T. Alexandrescu: Biochemistry **50** (2011) 2808.

15) H. Yagi, Y. Abe, N. Takayanagi, and Y. Goto: Biochim. Biophys. Acta. **1844** (2-14) 1881.

16) C. Goldsbury, P. Frey, V. Olivieri, U. Aebi, S. A. Müller: J. Mol. Biol. **352** (2005) 282.

17) M.Z. Kellermayer, Á. Karsai, M. Benke, K. Soós, and B. Penke: Proc. Natl. Acad. Sci. U. S. A. **105** (2008) 141.

18) P. -E. Milhiet, D. Yamamoto, O. Berthoumieu, P. Dosset, C. L. Grimellec, J.-M. Verdier, S. Marchal, and T. Ando: PLoS ONE **5** (2010) e13240.

19) H. Ogi, Y. Fukunishi, T. Omori, K. Hatanaka, M. Hirao, and M. Nishiyama: Anal. Chem. **80** (2008) 5494.

20) H. Ogi, M. Fukukshima, H. Hamada, K. Noi, M. Hirao, H. Yagi, and Y. Goto: Sci. Rep. **4** (2014) 6960.

21) R. H. Takahashi, T. A. Milner, F. Li, E. E. Nam, M. A. Edgar, H. Yamaguchi, M. F. Beal, H. Xu, P. Greengard, and G. K. Gouras: Am. J. Pathol. **161** (2002) 1869.

22) H. Ogi, H. Nagai,Y. Fukunishi, M. Hirao, and M. Nishiyama: Anal. Chem. **81** (2009) 8068.

23) H. Ogi: Proc. Jpn. Acad., Ser. B **89** (2013) 401.

24) R. Krishnan, J. L. Goodman, S. Mukhopadhyay, C. D. Pacheco, E. A. Lemke, A. A. Deniz, and S. Lindquist: Proc. Natl. Acad. Sci. U.S.A **109** (2012) 11172.

25) K. Yanagi, M. Ashizaki, H. Yagi, K. Sakurai, Y. H. Lee, and Y. Goto: J. Biol. Chem. **286** (2011) 23959.

26) K. Hasegawa, I. Yamaguchi, S. Omata, F. Gejyo, and H. Naiki: Biochemistry **38** (1999) 15514.

Figure Captions

Fig. 1. (Color online) Schematic of the TIRFM-QCM cell.

Fig. 2. (Color online) Changes of the resonance frequency of the quartz resonator and fibril-occupation area (upper), and corresponding TIRFM images (lower). The fibril occupation area was digitally computed, and three measurements at different areas are plotted by red circles. The scale bars in the TIRFM images indicate 5 μm.

Fig. 3. (Color online) TIRFM images at 0 h (a) and 5 h (b), and their merged image (c). Arrows point the initially immobilized seeds.

Fig. 4. (Color online) Two-color TIRFM images after the solution-flow measurement. The Nile-red image (a), the Th-T image (b), and their merged image (c) are shown. The scale bars indicate 5 μm.

Fig. 5. (Color online) Schematic explanation of the nucleation-fibrillation model on the quartz surface. The monomer solution is flowed alone the quartz surface, where the seeds are immobilized in advance (a). The oligomers are formed near the seeds (b), and nuclei occur inside the oligomer region (c). Many fibrils originate and grow from the nuclei, and some fibrils elongate from the initial seeds (d).

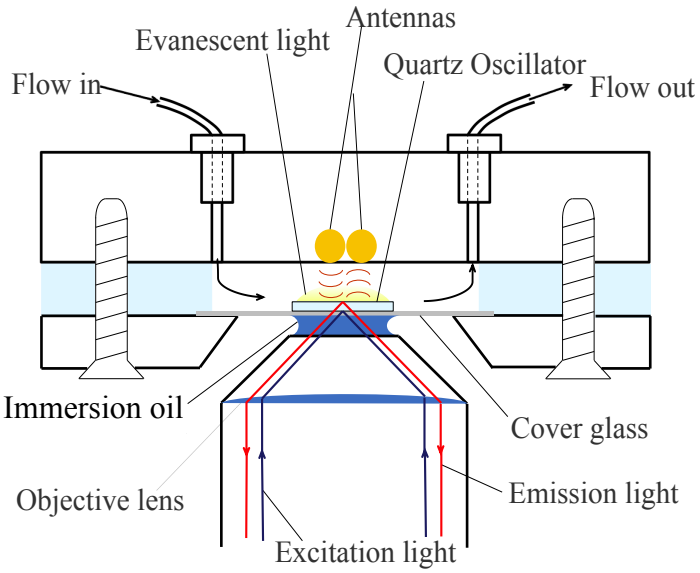
Antennas
Evanescent light
Quartz Oscillator
Flow in
Flow out
Immersion oil
Cover glass
Objective lens
Emission light
Excitation light

Fig. 1.

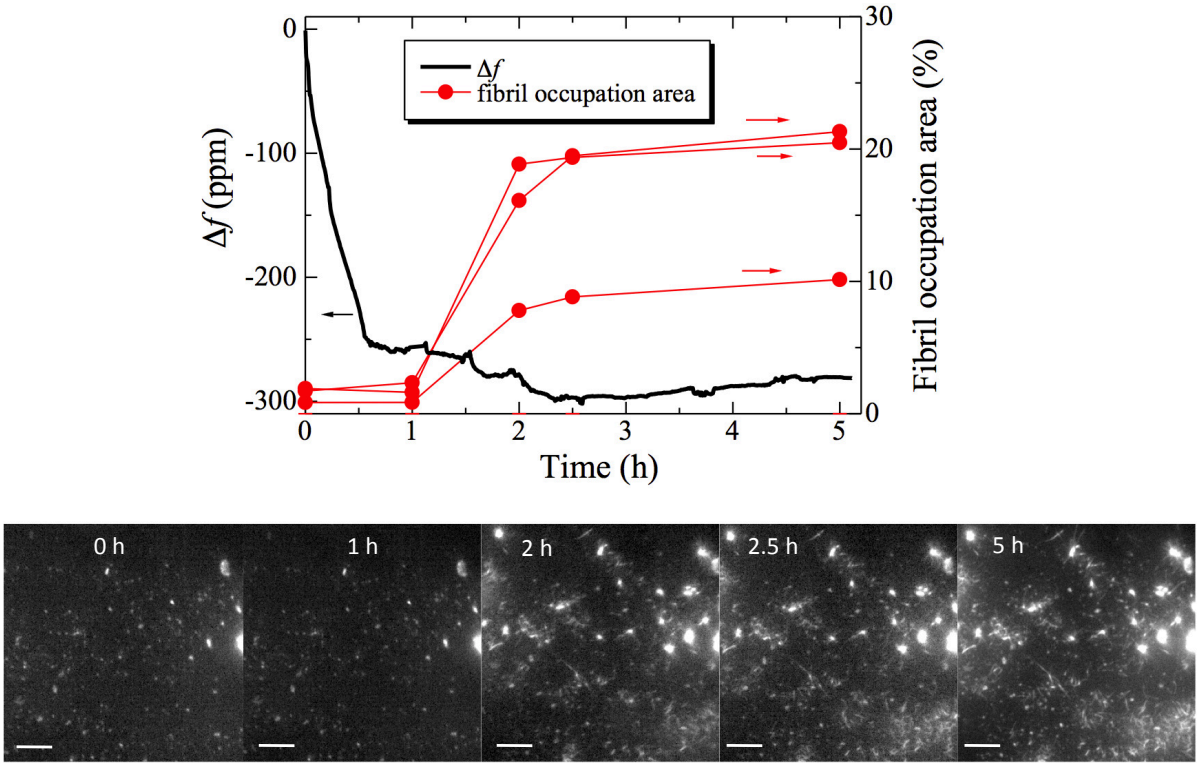
Δf
fibril occupation area
Δf (ppm)
Fibril occupation area (%)
Time (h)
0
-100
-200
-300
30
20
10
0
0
1
2
3
4
5
0 h
1 h
2 h
2.5 h
5 h

Fig. 2.

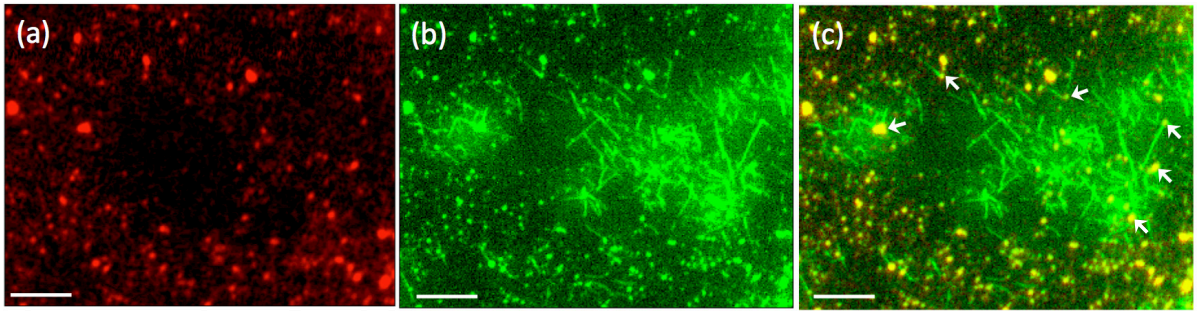

Fig. 3.

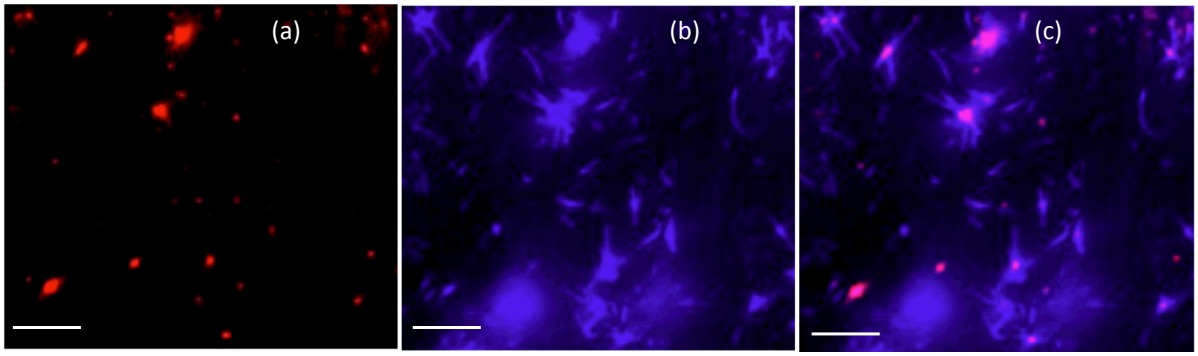

Fig. 4.

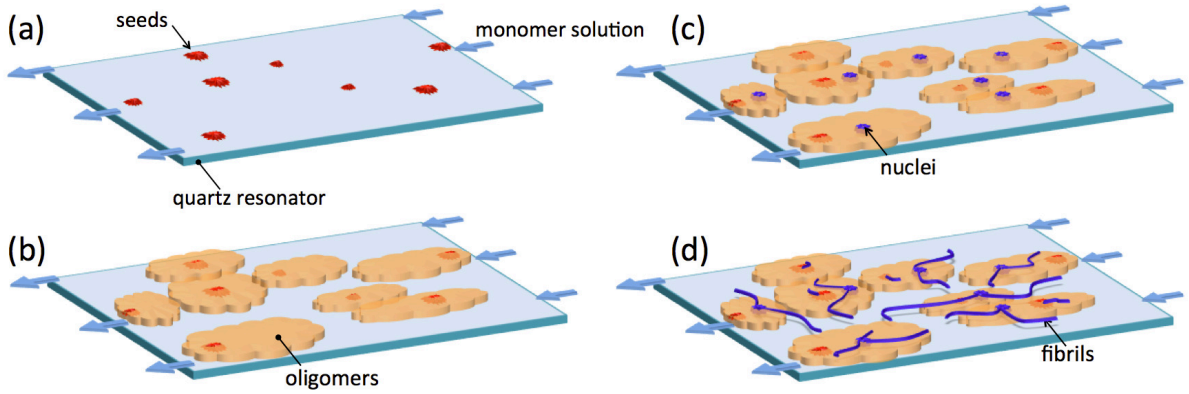
(a)
seeds
monomer solution
quartz resonator
(b)
oligomers
(c)
nuclei
(d)
fibrils

Fig. 5.